Article

Do Models beyond Hybrid Density Functionals Increase the Agreement with Experiment for Predicted NMR Chemical Shifts or Electric Field Gradient Tensors in Organic Solids?

Published as part of The Journal of Physical Chemistry virtual special issue "MQM 2022: The 10th Triennial Conference on Molecular Quantum Mechanics".

Robbie J. Iuliucci,* Joshua D. Hartman,* and Gregory J. O. Beran*

Cite This: https://doi.org/10.1021/acs.jpca.2c07657

Read Online

ACCESS | Metrics & More | Article Recommendations | SI Supporting Information

ABSTRACT: *Ab initio* predictions of chemical shifts and electric field gradient (EFG) tensor components are frequently used to help interpret solid-state nuclear magnetic resonance (NMR) experiments. Typically, these predictions employ density functional theory (DFT) with generalized gradient approximation (GGA) functionals, though hybrid functionals have been shown to improve accuracy relative to experiment. Here, the performance of a dozen models beyond the GGA approximation are examined for the prediction of solid-state NMR observables, including meta-GGA, hybrid, and double-hybrid density functionals and second-order Møller−Plesset perturbation theory (MP2). These models are tested on organic molecular crystal data sets containing 169 experimental ^{13}C and ^{15}N chemical shifts and 114 ^{17}O and ^{14}N EFG tensor components. To make these calculations affordable, gauge-including projector augmented wave (GIPAW) Perdew−Burke−Ernzerhof (PBE) calculations with periodic boundary conditions are combined with a local intramolecular correction computed at the higher level of theory. Within the context of typical NMR property calculations performed on a static, DFT-optimized crystal structure, the benchmarking finds that the double-hybrid DFT functionals produce errors versus experiment that are no smaller than those of hybrid functionals in the best cases, and they can be larger. MP2 errors versus experiment are even bigger. Overall, no practical advantages are found for using any of the tested double-hybrid functionals or MP2 to predict experimental solid-state NMR chemical shifts and EFG tensor components for routine organic crystals, especially given the higher computational cost of those methods. This finding likely reflects error cancellation benefiting the hybrid functionals. Improving the accuracy of the predicted chemical shifts and EFG tensors relative to experiment would probably require more robust treatments of the crystal structures, their dynamics, and other factors.
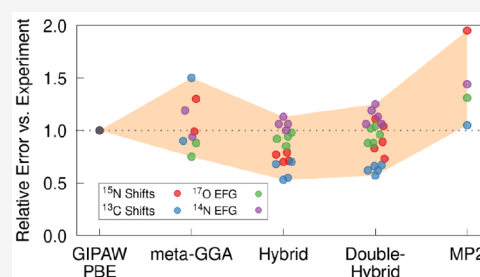
INTRODUCTION

Theoretical calculation of nuclear magnetic resonance (NMR) properties has become a widely used tool for facilitating the interpretation of NMR experiments. The sensitivity of NMR shielding constants and electric field gradient (EFG) tensors to the electronic environment makes them excellent probes of chemical structure. Still, this sensitivity also means that high-quality quantum mechanical models of the system are needed to predict the magnetic properties accurately. In organic crystals, the challenge of computing accurate chemical shieldings or EFG tensors is further complicated by the need to incorporate the influence of the crystal lattice. Over the past couple of decades, planewave density functional theory (DFT), which employs periodic boundary conditions to represent an infinite crystal, with the gauge-including projector augmented wave (GIPAW) approach has become the *de facto* standard method for modeling NMR properties of periodic systems due to its favorable balance between accuracy and computational cost.

Practical GIPAW calculations to date have largely been limited to generalized gradient approximation (GGA) functionals such as Perdew−Burke−Ernzerhof (PBE).[1] While there have been many successful applications of GIPAW PBE calculations for solid-state NMR problems,[2,3] more advanced hybrid functionals predict experimental chemical shifts for ^{13}C, ^{15}N, and ^{17}O with up to ~50% higher accuracy, depending on the nucleus type.[4−6] Similarly, hybrid density functionals can improve the accuracy of EFG tensor components by ~30%.[7] This raises the question of what further accuracy improvements might be obtained by using even higher-level electronic

A

structure models, such as double-hybrid density functionals or correlated wave function methods like second-order Møller−Plesset perturbation theory (MP2) and coupled cluster singles and doubles (CCSD). Double-hybrid density functionals exhibit superior performance over GGA and hybrid functionals for thermochemistry, noncovalent interactions, barrier heights, and conformational energies, for example.[8−11] Various studies on small systems have also demonstrated improvements in the absolute NMR shielding constants predicted with double-hybrid functionals, MP2, and CCSD instead of GGA or hybrid functionals.[12−16]

The benefits of employing such methods for practical prediction of experimental solid-state NMR chemical shifts or EFG tensors are less clear, however. The high computational cost of these approaches in the solid state has historically prevented large-scale testing of these methods for experimental chemical shift prediction in chemically interesting organic crystals. However, recent developments now make it computationally feasible to test these advanced models more broadly. First, the development of fast, density-fitted (a.k.a. resolution-of-the-identity) gauge-including atomic orbital (GIAO) and other algorithms for computing MP2 and double-hybrid density functional chemical shieldings in nonperiodic systems have lowered the computational costs by at least an order of magnitude compared to canonical MP2 algorithms.[14,17−21] The lower memory and disk storage requirements of these new algorithms also make them more practical to run on routine computer hardware.

Second, both finite molecular cluster models[4,22−24] and GIPAW calculations combined with a local, nonperiodic correction[6,7,25,26] have been shown to predict chemical shifts and electric field gradient (EFG) tensors in organic crystals with accuracy on par with or higher than standard GIPAW PBE results. A ~10−15 molecule cluster is often sufficient to reproduce chemical shifts in organic crystals,[22,23] especially when electrostatic embedding is employed to mimic the longer-range lattice contributions. The locally dense basis set approximation,[27,28] which employs larger basis sets on the central atoms/molecule(s) of interest in the cluster and fewer basis functions on more distant atoms, appreciably reduces the cost of computing the chemical shieldings in such clusters.

Further computational savings can be obtained using a fragment approach,[4,5,24,29,30] in which the single calculation on the full ~10−15 molecule cluster is replaced with a series of monomer and dimer calculations which capture the contributions from neighboring molecules incrementally in a pair-at-a-time fashion. In the hybrid many-body interaction (HMBI) one- and two-body fragment approach with self-consistent reproduction of the Madelung potential (SCRMP) embedding,[5] for example, one first computes a set of self-consistently polarized atomic point charges that are designed to reproduce the Madelung potential on the central monomer. Alternatively, a polarizable continuum model can also be used for electrostatic embedding.[31] One then computes the chemical shieldings for the central monomer embedded in this environment, followed by computing the shielding corrections to the monomer arising from dimers involving the central molecule and other nearby molecules lying within 4−6 Å of the central molecule. In other words, the SCRMP fragment approach replaces the calculation of the chemical shieldings in an infinite periodic crystal or in a large cluster with an embedded monomer and ~1−2 dozen embedded dimer calculations. A comparable many-body expansion approach has proved effective for EFG tensors as well.[26,32]

Benchmark SCRMP fragment calculations[5] of molecular crystal chemical shifts using the PBE functional perform about as well as GIPAW PBE for ^1H, ^{13}C, and ^{15}N. They give errors that are modestly larger for ^{17}O shifts, which are especially sensitive to the description of the electrostatic environment.[26] Switching to the hybrid PBE0 functional instead of PBE improves the accuracy of ^{13}C and ^{15}N chemical shifts by ~30−50% when using the HMBI SCRMP method. For example, the ^{13}C root-mean-square (rms) errors improved from 2.1 ppm with PBE to 1.1 ppm with PBE0.[5,6] Similar rms error improvement from 5.0 to 3.6 ppm was observed for ^{15}N. Comparable improvements have also been found when hybrid functionals are used instead of GGAs to predict the principal values for ^{13}C shielding tensors.[23,30] In NMR crystallography, such accuracy improvements can increase the discrimination between correct and incorrect candidate structures, for example.[33]

Alternatively, Dračínský et al. demonstrated how a simple, local gas-phase correction approach can be used to improve the quality of GIPAW GGA chemical shift predictions.[6] Subsequent work has extended this approach to EFG tensors.[7] Specifically, this "monomer-correction" approach starts with a standard periodic GIPAW PBE calculation. One then improves the chemical shielding of the molecule of interest in the crystal by computing a gas-phase correction for the shielding difference between the same GGA functional and a higher-quality model, such as hybrid PBE0. This approximation effectively amounts to modeling the isolated molecule at the higher level of theory, and using GIPAW PBE to compute how the gas-phase molecular chemical shielding is altered by the surrounding lattice. Because it involves only higher-level calculations on an isolated molecule, this monomer correction is inexpensive to compute. In benchmark testing, it produces errors comparable to or smaller than those of the finite cluster and fragment approaches. Embedding the gas-phase monomer-correction calculations in a polarizable continuum or SCRMP embedding model improves the accuracy even more.[25,26] Although they are beyond the scope of the present study, we also note that machine-learning (ML) approaches for NMR properties[34] can provide a computationally inexpensive alternative approach to improving accuracy. Of particular interest in the present context are ML methods that seek to improve lower-quality *ab initio* NMR calculations (Δ-ML)[35,36] or to use transfer learning[37,38] trained against a modest amount of experimental data to achieve much higher accuracy.

The combination of these advances means that it is now possible to apply methods like MP2 or double-hybrid density functionals to the calculation of solid-state NMR properties. Even with these methods, the computational cost of MP2 or double-hybrid density functional chemical shielding calculations remains much higher than those of GGA or hybrid functionals. This raises the question of whether such models improve the accuracy of predicting chemical shifts or EFG tensors relative to experiment sufficiently to justify the additional computational effort. The results from the literature are somewhat conflicting. A pair of smaller-scale studies on small gas-phase molecules[14] and ionic metal halides and chalcogenides (e.g., NaCl, LiBr, MgS, etc.)[39] found clear improvement in the predicted chemical shifts upon switching to MP2 or double-hybrid DFT. Shattenberg and Kaupp similarly found excellent performance for MP2 and double-hybrid functionals relative to coupled cluster benchmarks for a set of 372 light, main-group nuclear

shieldings,[15] Yan and Xu found similarly good performance for XYG3-type double-hybrid functionals for shielding constants and theoretical chemical shifts in small molecules and organics.[16]

In contrast, a large benchmark study of 148 experimental solution-phase ^{1}H chemical shifts found double-hybrid density functionals to produce errors that were similar to or larger than those from GGA or hybrid density functionals.[40] Dračínský et al. applied the local double-hybrid DFT, MP2, and CCSD gas-phase molecular corrections to GIPAW for a set of six small amino acid crystals.[41] They also found no meaningful chemical shift accuracy improvements from using MP2 or CCSD instead of PBE0, though they did observe the importance of spin−orbit and nuclear quantum effects, especially for protons in certain hydrogen bonding environments. Poidevin et al. obtained generally similar results on the same set of amino acids with cluster models and double-hybrid functionals.[42]

While these studies have all been very insightful, there has not yet been a broader study of the performance of MP2 or double-hybrid functionals for predicting experimental solid-state ^{13}C and ^{15}N chemical shifts in organic crystals. Nor has the performance of these models been investigated for other magnetic properties such as EFG tensor components. Here, we benchmark MP2, double-hybrid density functionals, and several other functionals on organic molecular crystal test sets containing 132 ^{13}C and 37 ^{15}N experimental chemical shifts, along with 81 ^{17}O and 33 ^{14}N experimental EFG tensor components. The primary purpose of these benchmarks is to assess, in the context of typical present-day solid-state computational NMR protocols which compute the NMR properties on a static, the DFT-optimized crystal structure, whether MP2 or double-hybrid functionals meaningfully improve the prediction of experimental NMR properties over simpler global hybrid functionals.

The benchmarks here find no clear practical benefit to using MP2 or double-hybrid functionals in predicting experimental chemical shifts or EFG tensors for ordinary organic crystals. Even if the more advanced models predict magnetic properties that are more faithful to high-level theoretical benchmarks, those improvements in the electronic structure treatment do not translate to improved agreement with experiment. Global hybrid functionals such as PBE0 provide comparable or superior accuracy versus experiment, and they do so with much greater computational efficiency. This conclusion likely stems in part from error cancellation and reflects the limitations of the standard solid-state computational NMR protocols, such as the neglect of dynamical averaging, nuclear quantum effects, etc. Nevertheless, it provides useful practical guidance for those seeking to compute experimental NMR chemical shifts or EFG tensors in organic crystals quickly and reliably.

COMPUTATIONAL METHODS

Chemical Shift Predictions. For consistency with previous work, the benchmark chemical shift calculations utilize molecular crystal test sets taken directly from ref 6. These sets consist of 132 experimental isotropic ^{13}C chemical shifts from 21 organic crystals and 37 ^{15}N chemical shifts from 16 crystals. The full list of species and Cambridge Structure Database reference codes is provided in Supporting Information Section 1.1. These molecular crystal test sets include amino acids, sugars, DNA bases, small drug molecules, and a handful of other small organics. The crystals primarily consist of neutral molecules composed of hydrogen, carbon, nitrogen, and oxygen, though a

small number of species also include sulfur, are salts with a chloride anion, and/or are zwitterionic. The local chemical environments in these test sets are sufficiently diverse that chemical shift referencing regression lines derived from them have proved transferable[4,5] and have enabled successful NMR crystallography studies in organic materials[33,43,44] and biological systems.[45−47]

The DFT-optimized crystal geometries were taken directly from ref 6. The geometry optimizations in that work were constrained to preserve the experimental lattice parameters, thereby capturing the finite-temperature thermal expansion in the crystals.[48] See ref 6 for further details. While one might seek to optimize the crystal structures at a higher level of theory, the use of GGA-optimized crystal structures is computationally expedient and widespread in computational NMR studies, making it a reasonable choice for the present benchmarks.

The monomer-correction approach evaluates the corrected chemical shielding σ_{MC} as

$$\sigma_{MC}^{High\text{-}Level} \approx \sigma_{crystal}^{GIPAW,PBE} - \sigma_{monomer}^{PBE} + \sigma_{monomer}^{High\text{-}Level} \tag{1}$$

where the first term on the right-hand side is the standard GIPAW PBE shielding, the second term is the gas-phase PBE shielding, and the third term represents the gas-phase shielding computed with a more advanced model such as a hybrid functional, double-hybrid functional, or MP2. The gas-phase monomer calculations are performed on the asymmetric unit in its crystalline geometry (i.e., directly extracted from the crystal with no change in geometry).

The GIPAW PBE chemical shieldings here were taken directly from ref 6. That study computed them in CASTEP 17.2, employing a 600 eV planewave cutoff, pseudopotentials generated "on the fly", and a Monkhorst−Pack k-point grid spacing of 0.05 Å^{-1}. Gas-phase chemical shieldings were calculated with PBE,[1] TPSS,[49] r^{2}SCAN,[50] PBE0,[51] B3LYP,[52] TPSS0,[53,54] ωB97M-V,[55] five double-hybrid functionals (PBE0-DH,[56] mPW2PLYP,[57] B2PLYP,[58] DSD-PBEP86,[59] and DSD-BLYP[60]), and MP2 using Orca 5.0.[61] Some of these double-hybrids have performed well in previous NMR chemical shielding studies.[14,39] The other functionals represent well-known meta-GGA, hybrid, hybrid meta-GGA, and range-separated hybrid meta-GGA functioanls.

"Tight" self-consistent field convergence criteria were used in Orca, and all electrons were correlated. The impact of basis set for the gas-phase molecular chemical shielding calculations was assessed across the cc-pVXZ (X = D, T, or Q),[62] cc-pwCVXZ (X = D or T),[63] and pcSseg-n basis sets (n = 1−3).[64] Based on the results from these nine basis sets (Supporting Information Section 1.2), the cc-pVTZ basis set was chosen for the remainder of the chemical shielding monomer-correction calculations unless otherwise specified. Some results in the 6-311+G(2d,p) basis set[65,66] are also reported for direct comparison with earlier studies. The density-fitting employed Orca's "AutoAux" automatic auxiliary basis set generation with default settings. In all cases, both the gas-phase monomer PBE and high-level shieldings in eq 1 are computed with the same basis set.

Some fragment-based calculations were also performed to help validate the monomer-corrected GIPAW results. Fragmentation of the molecular crystals was performed using the hybrid many-body interaction code,[67−69] including all dimers with nearest-atom intermolecular separations up to 6 Å. The monomer and dimer calculations were computed with Orca

and the methods described above. The conductor-like polarizable continuum model (CPCM)[70] was used for the electrostatic embedding of the monomer and dimer fragments, choosing ethanol parameters ($\epsilon \approx 25$) for the solvent. Previous work has demonstrated that the predicted chemical shifts are fairly insensitive to the specific choice of solvent dielectric, because the dielectric-dependent differences in chemical shielding largely cancel upon converting the chemical shieldings to chemical shifts.[31]

To compare against experimental chemical shifts, the *ab initio* chemical shieldings need to be properly referenced. Here, we employ the linear regression approach,

$$\sigma_i = \hat{m}\delta_i + \hat{b} \tag{2}$$

where σ_i is the absolute chemical shielding, δ_i is the chemical shift, and $\hat{m}$ and $\hat{b}$ are slope and intercept parameters determined via linear least-squares fitting against the experimental shifts. Separate regression parameters are fitted for each theoretical model chemistry (i.e., a given functional, basis set, etc.). The linear regression approach partially cancels systematic errors and can therefore reduce the performance differences between various models. On the other hand, linear regression referencing often improves agreement with experiment, can facilitate peak assignments, and is widely used in practical chemical shift prediction applications.[2,3,71,72] For these reasons, it is adopted here.

The quality of the resulting chemical shifts are assessed statistically by examining the residuals from the correlation plots with the metrics of mean absolute error (MAE), maximum absolute error (MaxAE), and root-mean-square deviations (RMSD). The precision of the experimental chemical shift measurements depends on both experimental parameters and sample conditions. Uncertainty, based on spectral line width, can be a small fraction of a ppm given fast magic angle spinning, high-power RF decoupling, and strong homogeneous magnetic fields. To address issues with peak assignments in multidimensional biomolecular solid-state NMR spectra, Tycko[73] reported the uncertainty in the isotropic chemical shifts to be less than 1/3 the line width, assuming good signal-to-noise. Line widths of 0.25 ppm are typical, though accidental overlap and broadening features can decrease the precision significantly. Cimetidine, one of the test set species here, can be used to demonstrate the upper bounds of experimental uncertainty. The line widths in the high-resolution ^{13}C spectrum of cimetidine[74] range from 39 to 140 Hz because of overlap and dipolar coupling to nitrogen. Acquired at 14.1 T, these ^{13}C line widths translate to 0.26 to 0.93 ppm, corresponding to an uncertainty of 0.1 to 0.3 ppm. In other words, the experimental uncertainties in the chemical shifts are an order of magnitude smaller than the errors obtained for the predicted chemical shifts. Significant additional errors in experimental solid state NMR chemical shifts can arise from the difficulties in referencing, incorrect shift assignments, or even the use of the wrong crystal form. While such issues cannot be entirely ruled out, the chemical shift data sets used here were previously curated with care, including performing new NMR experiments that revised questionable experimental data in several cases.[6]

Electric Field Gradient Calculations. The benchmark EFG tensor calculations utilize molecular crystal test sets adapted from previous ^{17}O and ^{14}N studies. The ^{17}O set is a subset of the crystals from ref 7 and consists of 81 ^{17}O EFG tensor components from 13 organic crystals. The set of 33 ^{14}N

EFG tensor components from eight crystals was adapted from ref 75 and ref 76. These molecular crystal test sets are composed of sugars, small drug molecules, nutraceutical compounds, amino acids, a DNA base, and other small molecules. The elemental composition of these sets is similar to that of the chemical shift test sets, albeit with a larger number of chloride salts. See Supporting Information Section 2.1 for the complete list of structures, Cambridge Crystallographic Database reference codes, and experimental EFG tensor values for the ^{17}O and ^{14}N test sets. The DFT-optimized crystal structures for the ^{17}O test set were taken from ref 7. The ^{14}N crystal structures were optimized here following the same protocol used for the ^{17}O structures.

The monomer correction for the EFG tensor is analogous to eq 1, replacing the chemical shift with the EFG tensor V as follows:

$$V_{MC}^{High\text{-}Level} \approx V_{crystal}^{GIPAW,PBE} - V_{monomer}^{PBE} + V_{monomer}^{High\text{-}Level} \tag{3}$$

where the first term is computed via a standard GIPAW calculation, the second term is the gas-phase PBE EFG tensor, and the third term is the gas-phase EFG tensor computed using a more advanced model. Just as described in eq 1, the gas-phase monomer calculations are performed on the asymmetric unit using the geometry extracted from the crystal structure.

The planewave EFG tensor calculations were computed using CASTEP 19.11,[77] with a 850 eV planewave cutoff, pseudopotentials generated "on the fly", and a Monkhorst−Pack k-point grid spacing of 0.05 Å^{-1}. Gas-phase monomer EFG tensor calculations were performed using either Gaussian 16[78] or Orca (and accounting for the opposite sign convention in the EFG tensors between the two codes) After testing the same nine basis sets as were examined for the chemical shifts (Supporting Information Section 2.2), the weighted core−valence Dunning cc-pwCVTZ basis set was adopted for all monomer-corrected EFG results below unless otherwise indicated. For comparison with the monomer-corrected values, EFG tensor calculations were also performed using a two-body fragment approach using SCRMP electrostatic embedding. Crystal fragmentation was performed using the hybrid many-body interaction (HMBI) code,[67−69] and two-body contributions were included from all dimers within 6 Å of the asymmetric unit.

Diagonalization of the EFG tensor yields three principal components defined such that $|V_{33}| \geq |V_{22}| \geq |V_{11}|$. Experimental EFG tensor components are obtained from two NMR observables and the fact that the EFG tensor is traceless. First, the nuclear quadrupolar coupling constant (C_q) is obtained from V_{33} according to

$$C_q = eQV_{33}/h \tag{4}$$

where e is the elementary charge, Q is the nuclear quadrupole moment, and h is Planck's constant. The nuclear quadrupole moment for ^{17}O is −25.58 and −20.44 mb for ^{14}N.[79] Second, the asymmetry parameter (η_q) represents the ratio of the difference in V_{11} and V_{22} to V_{33},

$$\eta_q = (V_{11} - V_{22})/V_{33} \tag{5}$$

These two NMR parameters can be extracted from the experimental NMR spectra via software simulation. The experimental C_q and η parameters for the crystal structures used here are provided in the Supporting Information. The

Table 1. Comparison of GIPAW, Monomer-Corrected GIPAW, and HMBI Chemical Shift Errors Relative to Experiment for the Data Set of 37 ^{15}N Chemical Shifts^a

Method	Basis Set	Error Statistics (ppm)			Regression	
		RMSE	MAE	MaxAE	Slope	Intercept
GIPAW PBE	600 eV	5.0	4.1	10.6	−0.9699	180.16
GIPAW PBE + meta-GGA Functional Correction						
TPSS	cc-pVTZ	5.0	3.6	8.6	−0.9170	180.87
r^{2}SCAN	cc-pVTZ	6.5	5.2	12.0	−0.8638	185.61
GIPAW PBE + Hybrid Functional Correction						
PBE0	6-311+G(2d,p)	3.5	2.9	9.1	−1.0187	189.16
PBE0	cc-pVTZ	3.5	2.9	9.2	−1.0203	189.40
B3LYP	cc-pVTZ	3.6	3.0	9.7	−1.0253	184.34
TPSS0	cc-pVTZ	3.9	3.2	7.6	−0.9777	190.15
ωB97M-V	cc-pVTZ	4.0	3.3	8.4	−1.0310	197.05
GIPAW PBE + Double-Hybrid Functional or MP2 Correction						
PBE0-DH	cc-pVTZ	3.7	3.0	7.9	−1.0228	196.30
mPW2PLYP	cc-pVTZ	4.2	3.3	12.4	−1.0020	193.18
B2PLYP	cc-pVTZ	4.5	3.6	13.6	−0.9873	191.90
DSD-PBEP86	cc-pVTZ	5.2	4.0	16.2	−0.9672	198.23
DSD-BLYP	cc-pVTZ	5.6	4.4	17.6	−0.9807	197.02
MP2	6-311+G(2d,p)	9.8	7.5	30.2	−0.9310	201.00
RI-MP2	cc-pVTZ	9.9	7.6	29.8	−0.9320	201.04
RI-MP2	cc-pVQZ	9.9	7.7	29.3	−0.9078	203.52
HMBI Fragment Approach						
PBE0 (SCRMP)	6-311+G(2d,p)	3.6	2.9	7.7	−0.9846	193.43
RI-MP2 (CPCM)	cc-pVTZ	9.8	7.6	33.3	−0.9171	206.42
PBE0-DH (CPCM)	cc-pVTZ	4.8	3.6	14.3	−0.9849	202.10

^{a}The regression parameters for eq 2 and statistical errors (in ppm) are shown.

calculations reported here focus on the errors in predicting the EFG tensor components V_{ii}.

RESULTS

Chemical Shifts. Previous benchmark chemical shift calculations on molecular crystals demonstrated how correcting periodic GIPAW PBE with a gas-phase molecular PBE0-correction according to eq 1 reduces the errors for ^{13}C and ^{15}N isotropic shifts by ∼30−50%.[6] Here, we investigate how the same strategy performs when methods like MP2 and various other functionals up to double-hybrid DFT are used for the monomer correction instead of the hybrid PBE0 functional. Consider first the 37 ^{15}N chemical shifts in 16 molecular crystals taken from ref 6. Table 1 reports the statistical performance measures and chemical shift regression parameters obtained from applying the monomer correction with a variety of different density functionals. Figure 1a contains colored box-and-whisker plots and gray kernel density estimates of the error distributions for the best-performing functionals of each type from Table 1: TPSS (meta-GGA), PBE0 (hybrid), TPSS0 (hybrid meta-GGA), PBE-DH (double-hybrid), mPW2PLYP (double-hybrid), and MP2. These are compared against GIPAW PBE and self-consistent reproduction of the Madelung potential (SCRMP) fragment PBE0/6-311+G(2d,p) calculations from ref 6.

GIPAW PBE predicts the experimental ^{15}N shifts in this test set with a root-mean-square error of 5.0 ppm. Ideally, employing more advanced DFT or MP2 models would reduce the rms errors relative to experiment. However, applying the monomer correction computed using either the TPSS (rmse 5.0 ppm) or r^{2}SCAN meta-GGA (rmse 6.5 ppm) does not lower the error relative to experiment. In contrast, performing the monomer correction with a hybrid functional like PBE0 or B3LYP reduces

the errors versus experiment appreciably, to 3.5−3.6 ppm. Correcting GIPAW with the hybrid meta-GGA TPSS0 or the range-separated hybrid meta-GGA ωB97M-V similarly improves agreement with experiment compared to either uncorrected GIPAW or the meta-GGA-corrected results, though their rms errors of 3.9−4.0 ppm are 10−15% larger than those obtained from PBE0 or B3LYP. These performance trends are consistent with our earlier fragment-based benchmark calculations of comparable functionals.[4]

Next, we examine how accurately MP2 and double-hybrid functionals reproduce these experimental chemical shifts in the monomer-corrected GIPAW approach. The MP2 monomer correction produces a large rms error of 9.9 ppm, which is double the error of uncorrected GIPAW. All five double-hybrid functionals tested in the monomer correction give rms errors versus experiment that are substantially smaller than those from MP2. PBE0-DH and mPW2PLYP produce the best rms errors of 3.7 and 4.2 ppm, respectively, while DSD-BLYP has the largest rms error of 5.6 ppm.

However, it is notable that none of these rms errors versus experiment is smaller than what is obtained from a PBE0 or B3LYP monomer correction (3.5−3.6 ppm), and two of the double-hybrid functionals give errors versus experiment that are slightly larger than results of the uncorrected GIPAW itself. The failure to obtain more accurate chemical shifts with the double-hybrid functionals is surprising, given previous studies that have demonstrated that double-hybrid functionals are more faithful to high-level benchmark absolute shielding constants (e.g., refs 14−16).

Correlated wave function methods like MP2 are generally more sensitive to basis set incompleteness than GGA or hybrid density functionals. To rule out the possibility that the results described above reflect errors stemming from inadequate basis
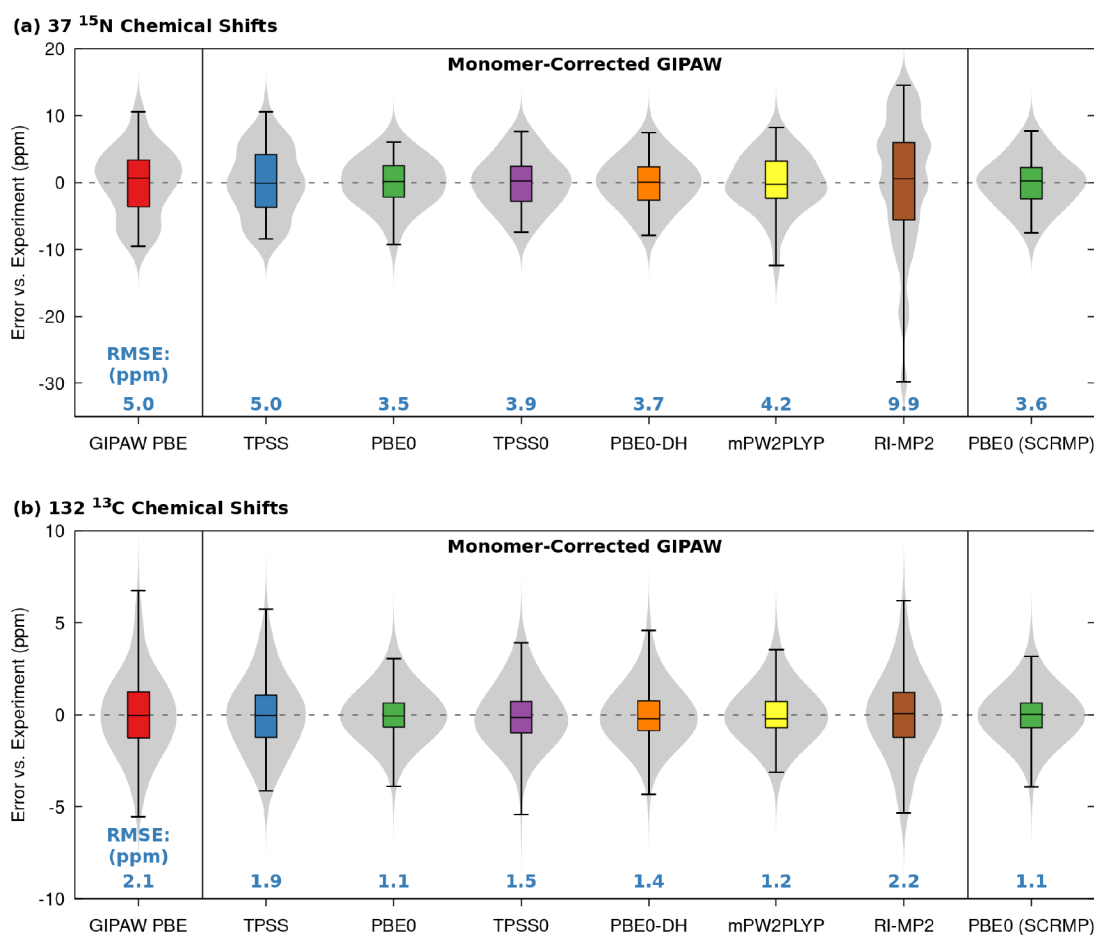
Figure 1. Error distributions relative to experiment for GIPAW PBE, HMBI-SCRMP PBE0, and several monomer-corrected GIPAW models in the (a) ^{15}N and (b) ^{13}C chemical shift data sets. The cc-pVTZ basis was used for the monomer corrections. The violins in gray show kernel density estimates of the error distributions. Box plots shown within each violin illustrate the median (black horizontal line), middle two quartiles (colored box), and outer quartile of data (whiskers).

sets in the monomer correction, the monomer-corrected shifts for PBE0, PBE0-DH, DSD-P86PBE, and MP2 were computed with nine different basis sets: 6-311+G(2d,p), the Dunning cc-pVXZ basis sets ranging from double- to quadruple-ζ, the weighted-core variant of the Dunning basis sets cc-pwCVDZ and cc-pwCVTZ (to test the impact of additional core basis functions), and Jensen's pcSseg-1, pcSseg-2, and pcSseg-3 (which were specifically designed for the computation of NMR properties). Consistent with previous work on PBE0-corrected GIPAW,[6] the choice of basis set employed in the monomer correction has only a minor impact on the statistical accuracy of the chemical shifts relative to experiment, especially for the smaller-error PBE0 and PBE0-DH models (Supporting Information Section 1.2). This insensitivity to basis set stems from the fact that some of the finite basis set error cancels when taking the difference between two functionals for the monomer correction, and from the additional cancellation of systematic error arising from the linear regression used to reference the chemical shifts.

The behavior of these models on the set of 132 ^{13}C isotropic shifts from 21 molecular crystals is qualitatively similar, as shown in Figure 1b and Table 2. The most notable differences are that the magnitude of the ^{13}C chemical shift errors are uniformly smaller than those for ^{15}N and that ^{13}C chemical shifts tend to be less sensitive to the model chemistry and electrostatic

environment. For this test set, GIPAW PBE gives an rms error of 2.1 ppm relative to experiment, and applying the TPSS meta-GGA monomer correction reduces the errors slightly to 1.9 ppm. In contrast, switching to the hybrid PBE0 functional using either the monomer correction or the SCRMP fragment approach reduces that by 45% to 1.1 ppm. The MP2 monomer correction once again performs rather poorly, with a 2.2 ppm rms error that is slightly larger than the original GIPAW PBE results. The rms errors for the five tested double-hybrid functionals range from 1.2−1.4 ppm, with mPW2PLYP performing the best and PBE0-DH and DSD-BLYP giving the largest errors (in contrast to the ^{15}N set, for which PBE0-DH was the best-performing double-hybrid functional). Although the double-hybrid functional monomer corrections clearly improve upon the GIPAW PBE ^{13}C test set chemical shifts relative to experiment, the rms errors obtained with the double-hybrid functionals are once again no smaller than those obtained with the much less expensive PBE0 or B3LYP hybrid functionals.

The lack of improvement for MP2 and double-hybrid functionals compared to simpler functionals motivated us to investigate the possibility that the results could be an artifact of monomer-corrected GIPAW PBE. First, we tried applying the monomer correction to GIPAW BLYP instead of GIPAW PBE for the ^{15}N chemical shift test set. Uncorrected GIPAW BLYP

Table 2. Comparison of GIPAW, Monomer-Corrected GIPAW, and HMBI Chemical Shift Errors Relative to Experiment for the Data Set of 132 ^{13}C Chemical Shifts[a]

Method	Basis Set	Error Statistics (ppm)			Regression	
		RMSE	MAE	Max AE	Slope	Intercept
GIPAW PBE	600 eV	2.1	1.6	6.8	−1.0044	170.44
GIPAW PBE + meta-GGA Functional Correction						
TPSS	cc-pVTZ	1.9	1.5	5.8	−0.9759	171.03
r^{2}SCAN	cc-pVTZ	3.1	2.1	11.3	−0.9402	172.66
GIPAW PBE + Hybrid Functional Correction						
PBE0	6-311+G(2d,p)	1.2	0.9	4.3	−1.0615	179.54
PBE0	cc-pVTZ	1.1	0.8	3.9	−1.0642	180.15
B3LYP	cc-pVTZ	1.2	0.9	3.2	−1.0533	173.08
TPSS0	cc-pVTZ	1.5	1.1	5.4	−1.0390	180.30
ωB97M-V	cc-pVTZ	1.4	1.0	5.0	−1.0786	183.04
GIPAW PBE + Double-Hybrid Functional or MP2 Correction						
PBE0-DH	cc-pVTZ	1.4	1.1	4.6	−1.0753	185.33
mPW2PLYP	cc-pVTZ	1.2	0.9	3.5	−1.0452	179.20
B2PLYP	cc-pVTZ	1.3	1.0	4.0	−1.0331	178.12
DSD-PBEP86	cc-pVTZ	1.3	1.0	3.8	−1.0292	183.59
DSD-BLYP	cc-pVTZ	1.4	1.1	4.0	−1.0334	181.95
RI-MP2	cc-pVTZ	2.2	1.7	6.2	−1.0003	183.95
HMBI Fragment Approach						
PBE0 (SCRMP)	6-311+G(2d,p)	1.1	0.8	3.9	−1.0336	185.71

[a]The regression parameters for eq 2 and statistical errors (in ppm) are shown.

gives an rms error of 5.8 ppm, compared to 5.0 ppm for GIPAW PBE (Supporting Information Section 1.3). However, the difference between the two baseline GIPAW functionals shrinks after applying the monomer correction, and the rms error trends for the different monomer-correction functionals mimic those from monomer-corrected GIPAW PBE. The primary difference is that the rms errors versus experiment are consistently ∼0.2−0.3 ppm larger when the monomer correction is applied to GIPAW BLYP instead of GIPAW PBE. See the Supporting Information for more details.

Second, one might question if the monomer-correction approach itself is problematic. Poidevin et al. presented data on a small set of amino acids in which large cluster QM/MM calculations with double-hybrid functionals gave improved agreement with experiment compared to a monomer correction on top of GGA cluster results.[42] Accordingly, we performed a set of fragment-based chemical shift calculations with MP2 and PBE0-DH on the ^{15}N crystal test set. These fragment calculations can be viewed as an approximate finite-cluster treatment of the crystals; no GIPAW GGA calculations are involved. The fragment calculations combine 1-body (intra-molecular) calculations and short-range two-body contributions (dimers up to 6 Å intermolecular separation), all electrostatically embedded in the CPCM implicit solvent model. The 1- and 2-body fragment approach with polarizable continuum model embedding has previously been shown to perform on par with the self-consistently polarized point-charge embedding used in the SCRMP model,[31] and the continuum embedding approach can be employed readily across different software packages.

As shown in Figure 1 and Table 1, monomer-corrected PBE0 and fragment-based SCRMP PBE0 both give ^{15}N rms errors in the 3.5−3.6 ppm range. Similar agreement between the two approaches is found for ^{13}C as well (Table 2). Figure 2 compares the ^{15}N error distributions between monomer-corrected and fragment calculations for MP2 and PBE0-DH. Although the fragment and monomer-corrected models vary in their chemical shift predictions for individual atoms, the two types of models
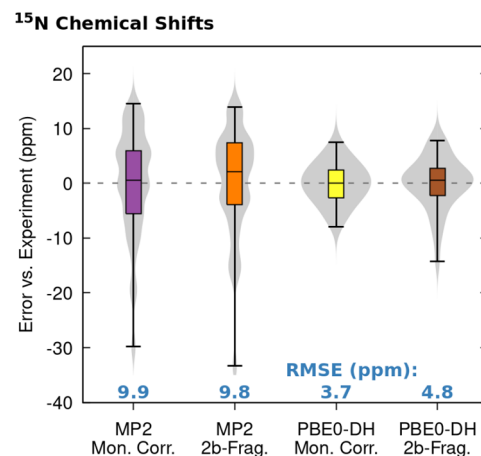

Figure 2. Comparison of the error distributions relative to experiment for 37 ^{15}N chemical shifts relative to experiment for MP2/cc-pVTZ and PBE0-DH/cc-pVTZ as computed with the monomer-corrected GIPAW and the 2-body fragment approaches.

give similar error distributions overall, regardless of whether MP2 or PBE0-DH is used. If anything, the monomer-corrected PBE0-DH results appear to benefit from error cancellation more so than the fragment-based ones. The results in Figure 2 suggest that the failure to obtain higher chemical shift accuracy with MP2 or the double-hybrid functionals is not an artifact of the GIPAW monomer-correction scheme.

Overall, the results presented here demonstrate that neither MP2 nor any of the five double-hybrid functionals tested predict ^{13}C and ^{15}N experimental chemical shifts with greater accuracy than the simpler PBE0 or B3LYP hybrid functionals. In some cases, the MP2 and double-hybrid errors are appreciably larger. This is particularly apparent in the ^{15}N chemical shifts, which tend to be more sensitive to the electronic structure treatment than ^{13}C. Before discussing potential reasons for these

Table 3. Comparison of GIPAW, Monomer-Corrected GIPAW, and HMBI EFG Tensor Components Relative to Experiment for the ^{17}O and ^{14}N Data Sets[a]

Method	Basis Set	^{17}O (MHz)			^{14}N (MHz)		
		RMSE	MAE	Max AE	RMSE	MAE	Max AE
GIPAW PBE	850 eV	0.48	0.39	1.56	0.16	0.13	0.35
GIPAW PBE + meta-GGA Functional Correction							
TPSS	cc-pwCVTZ	0.42	0.32	1.41	0.19	0.16	0.39
r^{2}SCAN	cc-pwCVTZ	0.36	0.26	1.26	0.15	0.12	0.31
GIPAW PBE + Hybrid Functional Correction							
PBE0	6-311+G(2d,p)	0.42	0.30	1.40	0.15	0.12	0.30
PBE0	cc-pwCVTZ	0.41	0.31	1.39	0.16	0.13	0.34
B3LYP	cc-pwCVTZ	0.45	0.33	1.47	0.17	0.14	0.34
TPSS0	cc-pwCVTZ	0.44	0.32	1.46	0.18	0.16	0.38
ωB97M-V	cc-pwCVTZ	0.47	0.35	1.61	0.17	0.14	0.32
GIPAW PBE + Double-Hybrid Functional or MP2 Correction							
PBE0-DH	cc-pwCVTZ	0.42	0.32	1.48	0.17	0.14	0.36
mPW2PLYP	cc-pwCVTZ	0.42	0.32	1.48	0.17	0.14	0.36
B2PLYP	cc-pwCVTZ	0.46	0.34	1.59	0.18	0.15	0.32
DSD-PBEP86	cc-pwCVTZ	0.50	0.38	1.70	0.20	0.15	0.45
DSD-BLYP	cc-pwCVTZ	0.49	0.38	1.70	0.19	0.15	0.41
RI-MP2	cc-pwCVTZ	0.63	0.51	1.87	0.23	0.15	0.57
HMBI Fragment Approach							
PBE (SCRMP)	6-311+G(2d,p)	0.57	0.47	1.68	0.18	0.12	0.47

[a]Statistical errors (in MHz) are provided for each nucleus.
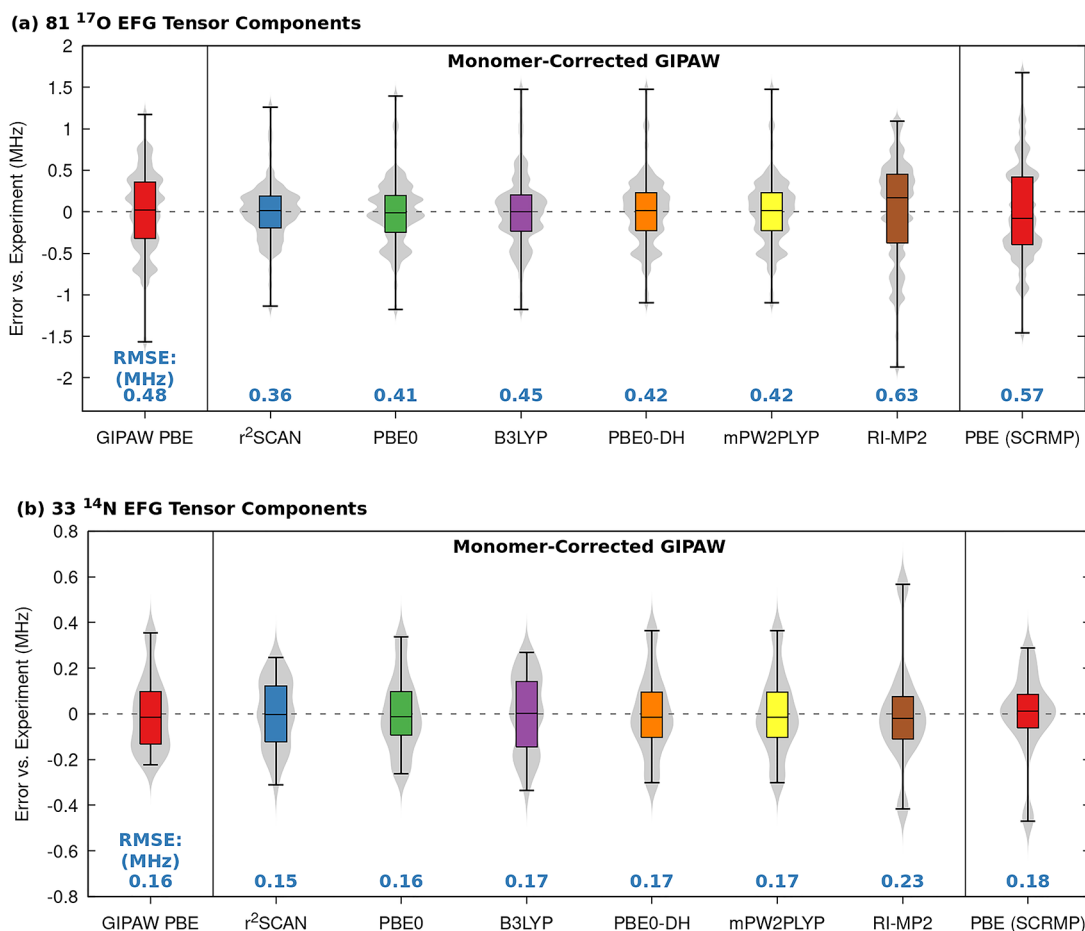

Figure 3. Error distributions relative to experiment for GIPAW PBE, HMBI-SCRMP PBE, and selected monomer-corrected GIPAW models using the (a) ^{17}O and (b) ^{14}N EFG tensor components data sets.

observations, the next section will first investigate the performance of these same models for EFG tensors.

Electric Field Gradient Tensor Components. Similar to chemical shieldings, EFG tensor components are sensitive to interactions with surrounding atoms. As a result, solid-state NMR involving the quadrupolar ^{17}O and ^{14}N nuclei provides an effective tool for examining structure and dynamics in complex systems.[80,81] Computational prediction of EFG tensors now plays a valuable role in extracting chemical insight from complex NMR spectra. Improving the accuracy of predicted EFG tensor components beyond GGA-based planewave techniques has been the subject of recent investigations. For example, fragment methods based on the many-body expansion approach have been successfully applied to ^{14}N EFG tensor calculations in molecular crystals.[32] Monomer-correction methods for GIPAW which employ hybrid density functionals have been shown to reduce the errors in predicted ^{17}O quadrupolar coupling constants by ~30% relative to uncorrected GIPAW calculations.[7,26] Here we extend these earlier studies by examining the accuracy of predicted ^{17}O and ^{14}N EFG tensor components obtained from monomer corrections performed using MP2 or double-hybrid density functionals. The complete list of EFG experimental tensor values and reported uncertainties are provided in the Supporting Information Section 2.3. The reported experimental uncertainties generally range 0.02−0.05 MHz (max 0.09 MHz) for ^{17}O, and 0.01−0.03 MHz for ^{14}N.

Table 3 summarizes the EFG tensor error statistics for of GIPAW PBE, PBE, with SCRMP embedding, and the various monomer-correction models. The violin plots in Figure 3 illustrate the error distributions for the best-performing functionals at each rung of Jacob's ladder. The results from two-body fragment calculations employing PBE with SCRMP embedding are included in this section for comparison with GIPAW PBE and previous work.[32] In agreement with previous ^{14}N studies, two-body fragment calculations yield comparable accuracy to GIPAW when the same PBE density functional is used.[32] Interestingly, two-body fragment SCRMP PBE calculations predict ^{17}O EFG tensor components that are rmse ~0.1 MHz less accurate than those obtained with GIPAW. Similar behavior has been found previously for isotropic ^{17}O chemical shifts, and it has been attributed to the high sensitivity of ^{17}O magnetic properties to the electrostatic environment.[4,26]

As previously observed for ^{17}O quadrupolar coupling constants,[7,26] a monomer correction performed at the PBE0 level modestly improves the accuracy of ^{17}O EFG tensor components. However, the 15% rms error reduction obtained for the full set of tensor components by applying the PBE0 monomer correction is about half the improvement seen previously for the ^{17}O quadrupolar coupling constants alone. On the other hand, the accuracy of predicted ^{14}N EFG tensor components is less sensitive to the monomer correction. The nominal improvement in accuracy observed for ^{14}N with the PBE0 monomer correction is within the experimental uncertainties of the EFG tensor data.

Looking at the other monomer-correction density functionals, the meta-GGA TPSS gives a 0.42 MHz rmse for ^{17}O, on par with the 0.41 MHz from PBE0, while the 0.19 MHz error for ^{14}N is a little larger than the 0.16 MHz for PBE0. In contrast, meta-GGA r^2SCAN gives smaller errors than any other functional tested for ^{17}O (rmse 0.36 MHz), while it is on par with PBE0 and many other methods for ^{14}N. This result contrasts the chemical shift test sets, for which the r^2SCAN rms errors were larger than those of any model except MP2. Similar to what was seen for the

chemical shift test sets, the other hybrid-type functionals (B3LYP, TPSS0, and ωB97M-V) give rmse errors that are mostly intermediate between GIPAW PBE and the PBE0-corrected GIPAW values.

Consider next the double-hybrid functionals. As discussed in Supporting Information Section 2.2, the double-hybrid functionals are more sensitive to the basis set used for the monomer correction than PBE0, with the inclusion of core basis functions being particularly important (consistent with earlier small molecule calculations of EFG tensors.[82]) For this reason, the cc-pwCVTZ set is used. We then find that the best-performing double-hybrid functionals PBE0-DH and mPW2PLYP again produce error statistics that are comparable to those from PBE0. The other three double-hybrids give rms errors that are on par with or slightly larger than those from GIPAW itself. That said, while the absolute DFT errors are several times larger than the experimental uncertainties, the relative statistical differences in rms error across different higher-level DFT functionals are often similar in magnitude to the experimental uncertainties. The largest outlier is MP2, which gives rms errors of 0.63 MHz for ^{17}O and 0.23 MHz for ^{14}N that are around 50% larger than the PBE0-corrected GIPAW errors. In summary, in the context of monomer-corrected GIPAW, neither MP2 nor any of the double-hybrid density functionals tested improves upon the hybrid PBE0 functional for predicting experimental ^{17}O and ^{14}N EFG tensor components in these test systems.

■ DISCUSSION

The benchmarks against experimental chemical shifts and EFG tensor elements performed here demonstrate a number of trends. While GIPAW PBE predicts these experimental properties fairly well, applying a monomer correction with a standard global hybrid functional such as PBE0 improves the accuracy of chemical shifts appreciably relative to experiment. Accuracy improvements for the EFG tensor elements relative to experiment are also observed, though they are more modest. The two best-performing double-hybrids identified here, PBE0-DH and mPW2PLYP, give statistical errors versus experiment for these properties that are similar to or slightly larger than those from PBE0-corrected GIPAW. Notably, however, none of the double-hybrid functionals produces errors that are smaller than those of PBE0, and some of the double-hybrids give errors that are no smaller than those of uncorrected GIPAW. MP2 often gives much larger errors than GIPAW PBE.

These results are perhaps surprising, given that previous studies have found double-hybrid DFT, and MP2 absolute chemical shieldings reproduce high-accuracy benchmarks more faithfully than lower-level DFT functionals.[12−16] It seems likely that considerable error cancellation is involved in the strong performance of basic hybrid functionals such as PBE0. Further evidence of error cancellation being involved comes from the work of Dračínský et al.,[41] who found that including spin−orbit and nuclear quantum effect corrections in their GIPAW + PBE0 results improved the accuracy of their ^{1}H chemical shifts relative to experiment, while decreasing the accuracy of their ^{13}C shifts. As the quality of the electronic structure treatment improves, other residual sources of errors that lead to disagreement with experiment may be manifesting more significantly.

This raises the question of what other sources of error might be obscuring whatever improvements are provided by double-hybrid functionals. The linear regression scheme used to reference the chemical shifts reduces systematic error in the absolute chemical shieldings. However, similar model perform-

ance trends occur for the EFG tensor predictions, which do not involve any regression or referencing. Errors in the GGA-level crystal geometries might be another contributing factor. For the 36 crystal structures taken from ref 6, 15-molecule clusters from each exhibit an excellent root-mean square deviation (rmsd15 metric[83]) of 0.053 Å on average. Thus, any geometry errors are small, though they could still reflect any systematic weaknesses inherent in dispersion-corrected GGA functionals. The use of single, static structures which neglect zero-point vibrational energy, dynamical averaging, and nuclear quantum effects is also likely a factor,[84−89] as may be the neglect of spin−orbit coupling.[41] Finally, the problems could lie within the density functionals themselves. It has been argued that magnetic field-dependent contributions to the correlation energy need to be included via current or magnetic field density functional theory[90−92] for high accuracy once good charge densities are achieved.[93]

Regardless of the fundamental reasons, the results here have important practical implications. The majority of present-day solid-state NMR modeling in organic crystals perform GIPAW or cluster calculations on a crystal structure that has been optimized with a dispersion-corrected GGA functional under periodic boundary conditions. In that context, a monomer correction to GIPAW at the level of PBE0 or a similar hybrid functional can reduce the errors versus experiment helpfully. However, there appears to be little additional practical benefit in terms of accuracy from applying the more expensive double-hybrid functionals, at least for routine organic crystals. MP2 should be avoided entirely in this context. Moreover, the computational cost of evaluating the monomer correction for a molecule like sucrose ($C_{12}H_{22}O_{11}$) with PBE0-DH is ∼15 times larger than with PBE0 (using Orca, the cc-pVTZ basis, 12 AMD EPYC 7282 cores, 60 GB RAM, and solid-state hard disk storage). That said, while the test sets used here include a variety of chemical species and elements, it would be interesting to examine how well these findings hold up for experimental shifts and EFG tensors in species containing a broader range of main group element or transition metal environments. Theoretical benchmarks suggest that main group elements can be more difficult to predict, for example.[15]

CONCLUSIONS

It is now possible to employ models such as MP2 and double-hybrid density functionals to predict chemical shifts and EFG tensors in organic solids, thanks to the combination of fast algorithms for computing MP2-like magnetic properties and approaches such as monomer-corrected GIPAW and fragment methods. While evidence from earlier studies indicates that methods beyond traditional GGA or hybrid density functionals can improve the description of absolute chemical shieldings, the benchmark calculations here find that neither MP2 nor any of the double-hybrid density functionals considered improve upon conventional hybrid density functionals for predicting experimental chemical shifts or EFG tensors in the monomer-corrected GIPAW approach. The errors versus experiment from MP2 are considerably larger than those from any of the DFT methods considered, while the double-hybrid functionals give errors that are at best on par with PBE0-corrected GIPAW and are sometimes closer in quality to uncorrected GIPAW PBE.

The apparent contradiction with the earlier benchmark studies against high-quality theoretical data suggests that error cancellation is probably a significant factor which favors functionals like PBE0 and that other limitations in typical computational NMR protocols prevent further accuracy improvements from the better electronic structure treatments. The most obvious limitation could lie in the use of static, GGA-optimized crystal geometries, instead of using higher-level functionals and accounting for vibrational dynamics and nuclear quantum effects. There could also be limitations in the monomer-correction approach, though the fragment-method tests here produced similar results.

Future work should continue investigating strategies for including these and other corrections and hopefully improving the overall accuracy of predicted NMR properties. That said, for routine studies which seek to predict solid-state NMR properties for typical organic crystals using DFT-optimized structures, the data here suggest that the extra computational expense associated with the use of MP2 or double-hybrid functionals does not translate to higher accuracy relative to experiment. Conventional hybrid functionals provide similar accuracy at much lower cost.

■ ASSOCIATED CONTENT

Ⓢ Supporting Information

The Supporting Information is available free of charge at https://pubs.acs.org/doi/10.1021/acs.jpca.2c07657.

Complete lists of the crystal structures included in the benchmark data sets; data tables of the predicted and experimental chemical shifts and EFG tensors; basis set convergence testing; impact of changing the baseline GIPAW functional; electric field gradient calculations; choice of basis set for the monomer correction; experimental and calculated quadrupole coupling constants (PDF)

DFT-optimized crystal structures for the EFG data sets (CIF)

■ AUTHOR INFORMATION

Corresponding Authors

Robbie J. Iuliucci − *Department of Chemistry, Washington and Jefferson College, Washington, Pennsylvania 15301, United States;* ⓘ orcid.org/0000-0001-6714-1842; Email: riuliucci@washjeff.edu

Joshua D. Hartman − *Department of Chemistry, University of California, Riverside, California 92521, United States;* Email: joshua.hartman@ucr.edu

Gregory J. O. Beran − *Department of Chemistry, University of California, Riverside, California 92521, United States;* ⓘ orcid.org/0000-0002-2229-2580; Email: gregory.beran@ucr.edu

Complete contact information is available at: https://pubs.acs.org/10.1021/acs.jpca.2c07657

Notes

The authors declare no competing financial interest.

■ ACKNOWLEDGMENTS

■ REFERENCES

(1) Perdew, J. P.; Burke, K.; Ernzerhof, M. Generalized gradient approximation made simple. *Phys. Rev. Lett.* **1996**, *77*, 3865.

(2) Bonhomme, C.; Gervais, C.; Babonneau, F.; Coelho, C.; Pourpoint, F.; Azaïs, T.; Ashbrook, S. E.; Griffin, J. M.; Yates, J. R.; Mauri, F.; et al. First-Principles Calculation of NMR Parameters Using the Gauge Including Projector Augmented Wave Method: A Chemist's Point of View. *Chem. Rev.* **2012**, *112*, 5733−5779.

(3) Ashbrook, S. E.; McKay, D. Combining Solid-State NMR Spectroscopy with First-Principles Calculations − A Guide to NMR Crystallography. *Chem. Commun.* **2016**, *52*, 7186−7204.

(4) Hartman, J. D.; Kudla, R. A.; Day, G. M.; Mueller, L. J.; Beran, G. J. O. Benchmark fragment-based ^{1}H, ^{13}C, ^{15}N and ^{17}O chemical shift predictions in molecular crystals. *Phys. Chem. Chem. Phys.* **2016**, *18*, 21686−21709.

(5) Hartman, J. D.; Balaji, A.; Beran, G. J. O. Improved electrostatic embedding for fragment-based chemical shift calculations in molecular crystals. *J. Chem. Theory Comput.* **2017**, *13*, 6043−6051.

(6) Dračínský, M.; Unzueta, P.; Beran, G. J. O. Improving the accuracy of solid-state nuclear magnetic resonance chemical shift prediction with a simple molecular correction. *Phys. Chem. Chem. Phys.* **2019**, *21*, 14992−15000.

(7) Hartman, J. D.; Mathews, A.; Harper, J. K. Fast and Accurate Electric Field Gradient Calculations in Molecular Solids With Density Functional Theory. *Frontiers in Chemistry* **2021**, *9*, 751711.

(8) Kozuch, S.; Martin, J. M. L. Spin-component-scaled double hybrids: An extensive search for the best fifth-rung functionals blending DFT and perturbation theory. *J. Comput. Chem.* **2013**, *34*, 2327−2344.

(9) Goerigk, L.; Hansen, A.; Bauer, C.; Ehrlich, S.; Najibi, A.; Grimme, S. A look at the density functional theory zoo with the advanced GMTKN55 database for general main group thermochemistry, kinetics and noncovalent interactions. *Phys. Chem. Chem. Phys.* **2017**, *19*, 32184−32215.

(10) Mardirossian, N.; Head-Gordon, M. Survival of the most transferable at the top of Jacob's ladder: Defining and testing the ωB97M(2) double hybrid density functional. *J. Chem. Phys.* **2018**, *148*, 241736.

(11) Martin, J. M.; Santra, G. Empirical Double-Hybrid Density Functional Theory: A 'Third Way' in Between WFT and DFT. *Isr. J. Chem.* **2020**, *60*, 787−804.

(12) Teale, A. M.; Lutnaes, O. B.; Helgaker, T.; Tozer, D. J.; Gauss, J. Benchmarking density-functional theory calculations of NMR shielding constants and spin-rotation constants using accurate coupled-cluster calculations. *J. Chem. Phys.* **2013**, *138*, 024111.

(13) Flaig, D.; Maurer, M.; Hanni, M.; Braunger, K.; Kick, L.; Thubauville, M.; Ochsenfeld, C. Benchmarking Hydrogen and Carbon NMR Chemical Shifts at HF, DFT, and MP2 Levels. *J. Chem. Theory Comput.* **2014**, *10*, 572−578.

(14) Stoychev, G. L.; Auer, A. A.; Neese, F. Efficient and Accurate Prediction of Nuclear Magnetic Resonance Shielding Tensors with Double-Hybrid Density Functional Theory. *J. Chem. Theory Comput.* **2018**, *14*, 4756−4771.

(15) Schattenberg, C. J.; Kaupp, M. Extended Benchmark Set of Main-Group Nuclear Shielding Constants and NMR Chemical Shifts and Its Use to Evaluate Modern DFT Methods. *J. Chem. Theory Comput.* **2021**, *17*, 7602−7621.

(16) Yan, W.; Xu, X. Accurate Prediction of Nuclear Magnetic Resonance Parameters via the XYG3 Type of Doubly Hybrid Density Functionals. *J. Chem. Theory Comput.* **2022**, *18*, 2931−2946.

(17) Gauss, J.; Werner, H.-J. NMR chemical shift calculations within local correlation methods: the GIAO-LMP2 approach. *Phys. Chem. Chem. Phys.* **2000**, *2*, 2083−2090.

(18) Loibl, S.; Schütz, M. NMR shielding tensors for density fitted local second-order Møller-Plesset perturbation theory using gauge including atomic orbitals. *J. Chem. Phys.* **2012**, *137*, 084107.

(19) Maurer, M.; Ochsenfeld, C. A linear- and sublinear-scaling method for calculating NMR shieldings in atomic orbital-based second-order Møller-Plesset perturbation theory. *J. Chem. Phys.* **2013**, *138*, 174104.

(20) Maurer, M.; Ochsenfeld, C. Spin Component-Scaled Second-Order Møller−Plesset Perturbation Theory for Calculating NMR Shieldings. *J. Chem. Theory Comput.* **2015**, *11*, 37−44.

(21) Stoychev, G. L.; Auer, A. A.; Gauss, J.; Neese, F. DLPNO-MP2 second derivatives for the computation of polarizabilities and NMR shieldings. *J. Chem. Phys.* **2021**, *154*, 164110.

(22) Holmes, S. T.; Iuliucci, R. J.; Mueller, K. T.; Dybowski, C. Density functional investigation of intermolecular effects on ^{13}C NMR chemical-shielding tensors modeled with molecular clusters. *J. Chem. Phys.* **2014**, *141*, 164121.

(23) Holmes, S. T.; Iuliucci, R. J.; Mueller, K. T.; Dybowski, C. Critical Analysis of Cluster Models and Exchange-Correlation Functionals for Calculating Magnetic Shielding in Molecular Solids. *J. Chem. Theory Comput.* **2015**, *11*, 5229−5241.

(24) Hartman, J. D.; Monaco, S.; Schatschneider, B.; Beran, G. J. O. Fragment-based ^{13}C nuclear magnetic resonance chemical shift predictions in molecular crystals: An alternative to plane-wave methods. *J. Chem. Phys.* **2015**, *143*, 102809.

(25) Hartman, J. D.; Harper, J. K. Improving the accuracy of GIPAW chemical shielding calculations with cluster and fragment corrections. *Solid State Nucl. Magn. Reson.* **2022**, *122*, 101832.

(26) Hartman, J. D.; Spock, L. E.; Harper, J. K. Benchmark accuracy of predicted NMR observables for quadrupolar 14N and 17O nuclei in molecular crystals. *Magn. Reson. Chem.* **2023**, DOI: 10.1002/mrc.5328.

(27) Chesnut, D. B.; Moore, K. D. Locally dense basis sets for chemical shift calculations. *J. Comput. Chem.* **1989**, *10*, 648−659.

(28) Chesnut, D. B.; Rusiloski, B. E.; Moore, K. D.; Egolf, D. A. Use of Locally Dense Basis Sets for Nuclear Magnetic Resonance Shielding Calculations. *J. Comput. Chem.* **1993**, *14*, 1364−1375.

(29) Hartman, J. D.; Beran, G. J. O. Fragment-based electronic structure approach for computing nuclear magnetic resonance chemical shifts in molecular crystals. *J. Chem. Theory Comput.* **2014**, *10*, 4862−4872.

(30) Hartman, J. D.; Beran, G. J. O. Accurate ^{13}C and ^{15}N molecular crystal chemical shielding tensors from fragment-based electronic structure theory. *Solid State Nucl. Magn. Reson.* **2018**, *96*, 10−18.

(31) Unzueta, P. A.; Beran, G. J. O. Polarizable continuum models provide an effective electrostatic embedding model for fragment-based chemical shift prediction in challenging systems. *J. Comput. Chem.* **2020**, *41*, 2251−2265.

(32) Gregorovič, A. The many-body expansion approach to ab initio calculation of electric field gradients in molecular crystals. *J. Chem. Phys.* **2020**, *152*, 124105.

(33) Hartman, J. D.; Day, G. M.; Beran, G. J. O. Enhanced NMR discrimination of pharmaceutically relevant molecular crystal forms through fragment-based ab initio chemical shift predictions. *Cryst. Growth Des.* **2016**, *16*, 6479−6493.

(34) Jonas, E.; Kuhn, S.; Schlörer, N. Prediction of chemical shift in NMR: A review. *Magn. Reson. Chem.* **2022**, *60*, 1021−1031.

(35) Gao, P.; Zhang, J. J.; Peng, Q.; Zhang, J. J.; Glezakou, V.-A. General Protocol for the Accurate Prediction of Molecular ^{13}C/^{1}H NMR Chemical Shifts via Machine Learning Augmented DFT. *J. Chem. Inf. Model.* **2020**, *60*, 3746−3754.

(36) Unzueta, P. A.; Greenwell, C.; Beran, G. J. O. Predicting density functional theory-quality nuclear magnetic resonance chemical shifts via Δ-machine learning. *J. Chem. Theory Comput.* **2021**, *17*, 826−840.

(37) Han, H.; Choi, S. Transfer Learning from Simulation to Experimental Data: NMR Chemical Shift Predictions. *J. Phys. Chem. Lett.* **2021**, *12*, 3662−3668.

(38) Guan, Y.; Shree Sowndarya, S. V.; Gallegos, L. C.; St. John, P. C.; Paton, R. S. Real-time prediction of ^{1}H and ^{13}C chemical shifts with DFT accuracy using a 3D graph neural network. *Chem. Sci.* **2021**, *12*, 12012−12026.

(39) Dittmer, A.; Stoychev, G. L.; Maganas, D.; Auer, A. A.; Neese, F. Computation of NMR Shielding Constants for Solids Using an Embedded Cluster Approach with DFT, Double-Hybrid DFT, and MP2. *J. Chem. Theory Comput.* **2020**, *16*, 6950−6967.

(40) de Oliveira, M. T.; Alves, J. M. A.; Braga, A. A. C.; Wilson, D. J. D.; Barboza, C. A. Do Double-Hybrid Exchange−Correlation Func-

tionals Provide Accurate Chemical Shifts? A Benchmark Assessment for Proton NMR. *J. Chem. Theory Comput.* **2021**, *17*, 6876−6885.

(41) Dračínský, M.; Vícha, J.; Bártová, K.; Hodgkinson, P. Towards Accurate Predictions of Proton NMR Spectroscopic Parameters in Molecular Solids. *ChemPhysChem* **2020**, *21*, 2075−2083.

(42) Poidevin, C.; Stoychev, G. L.; Riplinger, C.; Auer, A. A. High Level Electronic Structure Calculation of Molecular Solid-State NMR Shielding Constants. *J. Chem. Theory Comput.* **2022**, *18*, 2408−2417.

(43) Yang, C.; Zhu, L.; Kudla, R. A.; Hartman, J. D.; Al-Kaysi, R. O.; Monaco, S.; Schatschneider, B.; Magalhaes, A.; Beran, G. J. O.; Bardeen, C. J.; et al. Crystal structure of the meta-stable intermediate in the photomechanical, crystal-to-crystal reaction of 9-tertbutyl anthracene ester. *CrystEngComm* **2016**, *18*, 7319−7329.

(44) Chalek, K. R.; Dong, X.; Tong, F.; Kudla, R. A.; Zhu, L.; Gill, A. D.; Xu, W.; Yan, C.; Hartman, J. D.; Magalhaes, A.; et al. Bridging photochemistry and photomechanics with NMR crystallography: the molecular basis for the macroscopic expansion of an anthracene ester nanorod. *Chem. Sci.* **2021**, *12*, 453−463.

(45) Caulkins, B. G.; Young, R. P.; Kudla, R. A.; Yang, C.; Bittbauer, T. J.; Bastin, B.; Hilario, E.; Fan, L.; Marsella, M. J.; Dunn, M. F.; et al. NMR Crystallography of a Carbanionic Intermediate in Tryptophan Synthase: Chemical Structure, Tautomerization, and Reaction Specificity. *J. Am. Chem. Soc.* **2016**, *138*, 15214−15226.

(46) Holmes, J. B.; Liu, V.; Caulkins, B. G.; Hilario, E.; Ghosh, R. K.; Drago, V. N.; Young, R. P.; Romero, J. A.; Gill, A. D.; Bogie, P. M.; et al. Imaging active site chemistry and protonation states: NMR crystallography of the tryptophan synthase α-aminoacrylate intermediate. *Proc. Nat. Acad. Sci.* **2022**, *119*, No. e2109235119.

(47) Klein, A.; Rovo, P.; Sakhrani, V. V.; Wang, Y.; Holmes, J. B.; Liu, V.; Skowronek, P.; Kukuk, L.; Vasa, S. K.; Guntert, P.; Mueller, L. J.; Linser, R.; et al. Atomic-resolution chemical characterization of (2x)72-kDa tryptophan synthase via four- and five-dimensional 1 H-detected solid-state NMR. *Proc. Nat. Acad. Sci.* **2022**, *119*, No. e2114690119.

(48) McKinley, J. L.; Beran, G. J. O. Improving predicted nuclear magnetic resonance chemical shifts using the quasi-harmonic approximation. *J. Chem. Theory Comput.* **2019**, *15*, 5259−5274.

(49) Tao, J.; Perdew, J. P.; Staroverov, V. N.; Scuseria, G. E. TPSS: Climbing the Density Functional Ladder: Nonempirical Meta-Generalized Gradient Approximation Designed for Molecules and Solids. *Phys. Rev. Lett.* **2003**, *91*, 146401.

(50) Furness, J. W.; Kaplan, A. D.; Ning, J.; Perdew, J. P.; Sun, J. Accurate and Numerically Efficient r2SCAN Meta-Generalized Gradient Approximation. *J. Phys. Chem. Lett.* **2020**, *11*, 8208−8215.

(51) Adamo, C.; Barone, V. Toward reliable density functional methods without adjustable parameters: The PBE0 model. *J. Chem. Phys.* **1999**, *110*, 6158.

(52) Stephens, P. J.; Devlin, F. J.; Chabalowski, C. F.; Frisch, M. J. Ab initio calculation of vibrational absorption and circular dichroism spectra using density functional force fields. *J. Phys. Chem.* **1994**, *98*, 11623−11627.

(53) Staroverov, V. N.; Scuseria, G. E. Comparative assessment of a new nonempirical density functional: Molecules and hydrogen-bonded complexes. *J. Chem. Phys.* **2003**, *119*, 12129.

(54) Grimme, S. Accurate Calculation of the Heats of Formation for Large Main Group Compounds with Spin-Component Scaled MP2 Methods. *J. Phys. Chem. A* **2005**, *109*, 3067−3077.

(55) Mardirossian, N.; Head-Gordon, M. ωB97M-V: A combinatorially optimized, range-separated hybrid, meta-GGA density functional with VV10 nonlocal correlation. *J. Chem. Phys.* **2016**, *144*, 214110.

(56) Brémond, E.; Adamo, C. Seeking for parameter-free double-hybrid functionals: The PBE0-DH model. *J. Chem. Phys.* **2011**, *135*, 024106.

(57) Schwabe, T.; Grimme, S. Towards chemical accuracy for the thermodynamics of large molecules: new hybrid density functionals including non-local correlation effects. *Phys. Chem. Chem. Phys.* **2006**, *8*, 4398−4401.

(58) Grimme, S. Semiempirical hybrid density functional with perturbative second-order correlation. *J. Chem. Phys.* **2006**, *124*, 034108.

(59) Kozuch, S.; Martin, J. M. L. DSD-PBEP86: in search of the best double-hybrid DFT with spin-component scaled MP2 and dispersion corrections. *Phys. Chem. Chem. Phys.* **2011**, *13*, 20104.

(60) Kozuch, S.; Gruzman, D.; Martin, J. M. L. DSD-BLYP: A General Purpose Double Hybrid Density Functional Including Spin Component Scaling and Dispersion Correction. *J. Phys. Chem. C* **2010**, *114*, 20801−20808.

(61) Neese, F. The ORCA program system. *WIREs Comput. Mol. Sci.* **2012**, *2*, 73−78.

(62) Dunning, T. H. Gaussian basis sets for use in correlated molecular calculations. I. The atoms boron through neon and hydrogen. *J. Chem. Phys.* **1989**, *90*, 1007−1023.

(63) Peterson, K. A.; Dunning, T. H. Accurate correlation consistent basis sets for molecular core−valence correlation effects: The second row atoms Al−Ar, and the first row atoms B−Ne revisited. *J. Chem. Phys.* **2002**, *117*, 10548−10560.

(64) Jensen, F. Segmented Contracted Basis Sets Optimized for Nuclear Magnetic Shielding. *J. Chem. Theory Comput.* **2015**, *11*, 132−138.

(65) Krishnan, R.; Binkley, J. S.; Seeger, R.; Pople, J. A. Self-consistent molecular orbital methods. XX. A basis set for correlated wave functions. *J. Chem. Phys.* **1980**, *72*, 650−654.

(66) Frisch, M. J.; Pople, J. A.; Binkley, J. S. Self-consistent molecular orbital methods 25. Supplementary functions for Gaussian basis sets. *J. Chem. Phys.* **1984**, *80*, 3265−3269.

(67) Beran, G. J. O. Approximating quantum many-body intermolecular interactions in molecular clusters using classical polarizable force fields. *J. Chem. Phys.* **2009**, *130*, 164115.

(68) Beran, G. J. O.; Nanda, K. Predicting organic crystal lattice energies with chemical accuracy. *J. Phys. Chem. Lett.* **2010**, *1*, 3480−3487.

(69) The HMBI software can be downloaded at https://github.com/gberan/HMBI.

(70) Barone, V.; Cossi, M. Quantum Calculation of Molecular Energies and Energy Gradients in Solution by a Conductor Solvent Model. *J. Phys. Chem. A* **1998**, *102*, 1995−2001.

(71) Lodewyk, M. W.; Siebert, M. R.; Tantillo, D. J. Computational Prediction of 1 H and 13 C Chemical Shifts: A Useful Tool for Natural Product, Mechanistic, and Synthetic Organic Chemistry. *Chem. Rev.* **2012**, *112*, 1839−1862.

(72) Beran, G. J. O. Calculating nuclear magnetic resonance chemical shifts from density functional theory: A primer. *eMagRes.* **2019**, *8*, 215−226.

(73) Tycko, R. On the problem of resonance assignments in solid state NMR of uniformly 15N,13C-labeled proteins. *J. Magn. Reson.* **2015**, *253*, 166−172.

(74) Holmes, S. T.; Engl, O. G.; Srnec, M. N.; Madura, J. D.; Quiñones, R.; Harper, J. K.; Schurko, R. W.; Iuliucci, R. J. Chemical Shift Tensors of Cimetidine Form A Modeled with Density Functional Theory Calculations: Implications for NMR Crystallography. *J. Phys. Chem. A* **2020**, *124*, 3109−3119.

(75) Holmes, S. T.; Hook, J. M.; Schurko, R. W. Nutraceuticals in Bulk and Dosage Forms: Analysis by ^{35}Cl and ^{14}N Solid-State NMR and DFT Calculations. *Mol. Pharm.* **2022**, *19*, 440−455.

(76) Giavani, T.; Bildsøe, H.; Skibsted, J.; Jakobsen, H. J. A solid-state ^{14}N magic-angle spinning NMR study of some amino acids. *J. Magn. Reson.* **2004**, *166*, 262−272.

(77) Clark, S. J.; Segall, M. D.; Pickard, C. J.; Hasnip, P. J.; Probert, M. I.; Refson, K.; Payne, M. C. First principles methods using CASTEP. *Z. für Krist.—Cryst. Mater.* **2005**, *220*, 567−570.

(78) Frisch, M. J.; Trucks, G. W.; Schlegel, H. B.; Scuseria, G. E.; Robb, M. A.; Cheeseman, J. R.; Scalmani, G.; Barone, V.; Petersson, G. A.; Nakatsuji, H.; et al. *Gaussian~16* Revision C.01; Gaussian Inc.: Wallingford, CT, 2016.

(79) Pyykkö, P. Spectroscopic nuclear quadrupole moments. *Mol. Phys.* **2001**, *99*, 1617−1629.

(80) Shen, J.; Terskikh, V.; Struppe, J.; Hassan, A.; Monette, M.; Hung, I.; Gan, Z.; Brinkmann, A.; Wu, G. Solid-state ^{17}O NMR study of α-d-glucose: exploring new frontiers in isotopic labeling, sensitivity

enhancement, and NMR crystallography. *Chem. Sci.* **2022**, *13*, 2591−2603.

(81) Duong, N. T.; Nishiyama, Y. Detection of remote proton−nitrogen correlations by 1 H-detected ^{14}N overtone solid-state NMR at fast MAS. *Phys. Chem. Chem. Phys.* **2022**, *24*, 10717−10726.

(82) Harbison, G. S. Polarization of core orbitals and computation of nuclear quadrupole coupling constants using Gaussian basis sets. *J. Magn. Reson.* **2015**, *257*, 24−31.

(83) Chisholm, J. A.; Motherwell, W. D. S. COMPACK: A program for identifying crystal structure similarity using distances. *J. Appl. Crystallogr.* **2005**, *38*, 228−231.

(84) Dumez, J.-N.; Pickard, C. J. Calculation of NMR chemical shifts in organic solids: Accounting for motional effects. *J. Chem. Phys.* **2009**, *130*, 104701.

(85) Dračínský, M.; Hodgkinson, P. A molecular dynamics study of the effects of fast molecular motions on solid-state NMR parameters. *CrystEngComm* **2013**, *15*, 8705.

(86) Dračínský, M.; Möller, H. M.; Exner, T. E. Conformational Sampling by Ab Initio Molecular Dynamics Simulations Improves NMR Chemical Shift Predictions. *J. Chem. Theory Comput.* **2013**, *9*, 3806−3815.

(87) Dračínský, M.; Hodgkinson, P. Effects of Quantum Nuclear Delocalisation on NMR Parameters from Path Integral Molecular Dynamics. *Chem.—Eur. J.* **2014**, *20*, 2201−2207.

(88) Dračínský, M.; Bouř, P.; Hodgkinson, P. Temperature Dependence of NMR Parameters Calculated from Path Integral Molecular Dynamics Simulations. *J. Chem. Theory Comput.* **2016**, *12*, 968−973.

(89) Engel, E. A.; Kapil, V.; Ceriotti, M. Importance of Nuclear Quantum Effects for NMR Crystallography. *J. Phys. Chem. Lett.* **2021**, *12*, 7701−7707.

(90) Vignale, G.; Rasolt, M. Density-functional theory in strong magnetic fields. *Phys. Rev. Lett.* **1987**, *59*, 2360−2363.

(91) Vignale, G.; Rasolt, M. Current- and spin-density-functional theory for inhomogeneous electronic systems in strong magnetic fields. *Phys. Rev. B* **1988**, *37*, 10685−10696.

(92) Grayce, C. J.; Harris, R. A. Magnetic-field density-functional theory. *Phys. Rev. A* **1994**, *50*, 3089−3095.

(93) Reimann, S.; Borgoo, A.; Tellgren, E. I.; Teale, A. M.; Helgaker, T. Magnetic-Field Density-Functional Theory (BDFT): Lessons from the Adiabatic Connection. *J. Chem. Theory Comput.* **2017**, *13*, 4089−4100.